Zhaoqi Yin, Yunfeng Han, Yingyu Ren, Qiuyi Yang and Ningde Jin*

Nonlinear Dynamic Characteristics of Oil-in-Water Emulsions

DOI 10.1515/zna-2016-0157
Received April 18, 2016; accepted May 21, 2016; previously published online June 14, 2016

Abstract: In this article, the nonlinear dynamic characteristics of oil-in-water emulsions under the addition of surfactant were experimentally investigated. Firstly, based on the vertical upward oil–water two-phase flow experiment in 20 mm inner diameter (ID) testing pipe, dynamic response signals of oil-in-water emulsions were recorded using vertical multiple electrode array (VMEA) sensor. Afterwards, the recurrence plot (RP) algorithm and multi-scale weighted complexity entropy causality plane (MS-WCECP) were employed to analyse the nonlinear characteristics of the signals. The results show that the certainty is decreasing and the randomness is increasing with the increment of surfactant concentration. This article provides a novel method for revealing the nonlinear dynamic characteristics, complexity, and randomness of oil-in-water emulsions with experimental measurement signals.

Keywords: Dynamic Characteristics; Nonlinear Analysis; Oil-in-Water Emulsions; Surfactant.

1 Introduction

Emulsions are widely encountered in food, pharmaceutical products, cleaning, and oil industry. In particular, about 80 % of exploited crude oil is in a state of emulsions. Understanding the dynamic characteristics of emulsions is of great significance to explore the mechanism of chemical flooding and the production characteristics of oil well. With the addition of surfactant, the interfacial tension of oil–water mixtures can be greatly reduced. So far, the phase slippage, droplet concentration, and velocity distribution of emulsions are not clarified. Therefore, it is urgent to reveal the dynamic characteristics of emulsions from the experimental measurement and theoretical analysis.

Emulsions stability can be described through morphological properties, electrical properties, and interfacial properties. Stratification of emulsions can be adopted to describe the morphological properties of emulsions quantitatively. The emulsions become less stable with the creaming rate increasing [1]. The stability of emulsions can also be investigated by droplet size distribution and the change of droplet size versus time. The characteristics of the droplet size are mainly obtained by microscopic observation [2–4], light scattering [5], and nuclear magnetic resonance [6, 7]. As the crude oil emulsion is composed of a variety of natural active substances and additives, the interaction between the components can cause the variations of electrical properties of emulsions [8–10]. The interfacial film between oil and water is used to describe the interface property of emulsions, and the presence of interfacial film hinders the emulsion coalescence, which stabilises the emulsions. The strength of interfacial molecular film can be characterised through measuring interfacial tension [10–12] and interfacial rheological properties [13–16]. However, previous studies on the stability of emulsions are limited in static experiment measurement and analysis, and the knowledge of the stability of flowing emulsions is very deficient. To a certain extent, it has restricted the choice of methods for measuring flow parameters of emulsions. Currently, the studies on gas–liquid two-phase flow under the addition of surfactant are mainly confined to the variation of flow pattern, pressure gradient, and liquid holdup [17–20]. In addition, the effect of water fraction on the stability of water-in-oil emulsions has also been reported [21].

Despite great breakthrough has been made in researches on emulsion properties under the addition of surfactant, literatures on reporting the dynamic characteristics of oil-in-water emulsions are still very limited. As a measure of system complexity and regularity, entropy is an important parameter characterising the complexity of nonlinear dynamic system. Bandt and Pompe [22] proposed permutation entropy, through which the system complexity was described by the statistical phase space vector arrangement. This algorithm is easy to implement

***Corresponding author: Ningde Jin,** School of Electrical Engineering and Automation, Tianjin University, Tianjin 300072, China, Tel./Fax: +86-22-27407641, E-mail: ndjin@tju.edu.cn
Zhaoqi Yin, Yunfeng Han, Yingyu Ren and Qiuyi Yang: School of Electrical Engineering and Automation, Tianjin University, Tianjin 300072, China

and possesses better robustness. Furthermore, it also presents better ability to distinguish the typical chaotic signals and random ones [23]. Fadlallah et al. [24] propounded a weighted permutation entropy algorithm, which can effectively preserve the original information of time series and improve the anti-noise ability as well as signal resolution. Chen et al. [25] developed the weighted permutation entropy to the multi-scale analysis of time series and found that multi-scale weighted permutation entropy (MS-WPE) exhibits a more significant anti-noise ability and signal resolution than weighted permutation entropy. The method of complexity entropy causality plane (CECP) was introduced by Rosso et al. [26, 27] to investigate the system characteristics with entropy and nonequilibrium. The CECP method is generalised to the multi-scale analysis of time series (MS-CECP) by Dou et al. [28]. They reported that MS-CECP enriches the understanding on the stability of flow pattern and system dynamic structure. Tang et al. [29] combined MS-CECP with MS-WPE and put forward the multi-scale weighted complexity entropy causality plane (MS-WCECP) and employed it on the investigation of gas–liquid two-phase flow. The results demonstrate that MS-WCECP can not only reflect the complexity of the nonlinear dynamic system but also uncover the certainty and randomness of the flow structure in detail.

This study focuses on the dynamic characteristics of flowing oil-in-water emulsions in vertical upward oil–water two-phase flow experiment under the addition of anionic surfactant sodium dodecyl benzene sulfonate (SDBS). Firstly, dynamic response signals of oil-in-water emulsions sampled by vertical multiple electrode array (VMEA) sensor were acquired in flow loop facility and sensor system in Tianjin University. The fluctuation signals were analysed by recurrence plot (RP) algorithm and multi-scale weighted complexity entropy causality plane (MS-WCECP) method, based on which we found that the results using the two methods aforementioned show satisfied consistency. This study provides an effective and novel perspective for the analysis of dynamic characteristics of oil-in-water emulsions.

2 Experiments and Data Acquisition of Oil-in-Water Emulsions

The experiment was carried out in flow loop facility and sensor system in Tianjin University. The facility consists of a surfactant aqueous solution tank (named water tank in the following), an oil tank, two peristaltic pumps, testing pipe, and a mixing tank. In the experiment, oil phase and surfactant aqueous solution were pumped out from oil tank and water tank, respectively. Then, the mixture of oil and surfactant aqueous solution was introduced into vertical upward pipe. Besides, the VMEA sensor installed on the testing pipe is used to measure dynamic response signals of oil-in-water emulsions. Finally, the emulsions are drained to the mixing tank.

Figure 1 shows the flow loop facility for oil–water two-phase flow experiment. The length and ID of testing pipe are 1600 and 20 mm, respectively. The vertical VMEA sensor is installed at the height of 1000 mm from the inlet to ensure full development, of which the length is 150 mm. Before the experiment, different proportions of water and surfactant were mixed together and stirred in the blender to obtain two concentrations of surfactant aqueous solutions (0.1 %wt, 0.25 %wt). Then, the water-cut was firstly fixed with increasing the total flow velocity, and dynamic response signals of VMEA sensor were acquired at different flow conditions. The water-cut (K_w) is set at 80 %, 84 %, 88 %, 92 %, and 96 %, whereas the total flow velocity U_m of oil and surfactant aqueous solutions ranges from 0.0184 to 0.2576 m/s.

The mediums including surfactant, water, and oil used in the experiment are SDBS, tap water, and No. 3 industry white oil, respectively. SDBS is a white powdery solid, non-volatile, and soluble in water and classified as anion surfactant. The densities of the oil and water phase at 20 °C are 801 and 1000 kg/m^3, respectively.

Figure 2 illustrates the measurement system of VMEA sensor, which consists of VMEA sensor, constant voltage AC excitation source module, signal conditioning module,

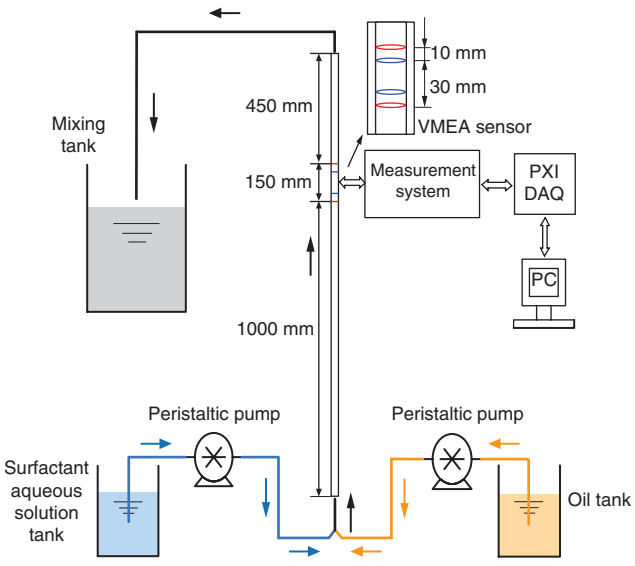

Figure 1: Flow loop facility for oil–water two-phase flow experiment.

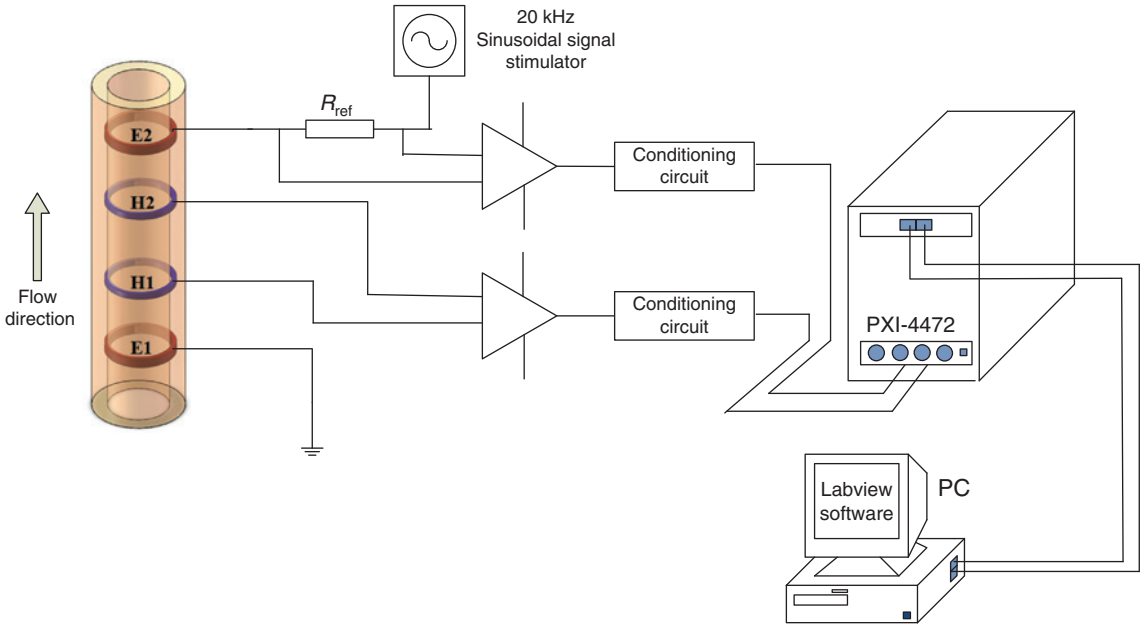

Figure 2: Measurement system of VMEA sensor.

and a data acquisition system based on PXI bus. In Figure 2, electrode E_1 is grounding, whereas electrode E_2 is an exciting electrode and stimulated by a 2 kHz sinusoidal signal. Electrodes H_1 and H_2 are measurement electrodes. The excitation source will generate a sinusoidal signal with constant voltage at a frequency of 2 kHz. It connects the electrode E_2 through reference resistance R_{ref} to stimulate the electrical field of sensor. The voltages of reference resistance R_{ref} and electrode H_1–H_2 are difference amplified and processed by signal conditioning module. Then, the reference voltage V_{ref} and the output voltage V_m of sensor are recorded by data acquisition card PXI 4472 of NI Corporation. Finally, the signals are collected in the computer. The sampling frequency is 2 kHz, and the sampling time is set as 30 s.

The characteristics of emulsion under the pipeline flow have received less attention. Al-Yaari et al. [21] studied the flow characteristics of water-in-oil emulsion in the horizontal pipe, and an optical microscope was utilised in the experiment to capture the droplet size distribution at different water volume fractions. The result indicates that the droplet size of dispersed phase is decreasing and the emulsion is more stable with the increasing water volume fraction, the maximum value of which is set not more than 70 % regarding their description. Meanwhile, this literature also proved the availability of observing emulsions using imaging method. Therefore, the droplet size distribution of emulsion with surfactant concentration of 0.25 %wt and water-cut being more than 80 % was observed and recorded by an optical microscope in this study.

Figure 3a, c, e, and g illustrates the images corresponding to total flow velocities set as 0.0184, 0.0736, 0.1840, and 0.2576 m/s with water-cut of 80 %, respectively, whereas Figure 3b, d, f, and h exhibits the photographs of total flow velocities selected as 0.0184, 0.0736, 0.1840, and 0.2576 m/s with water-cut being 96 %, respectively. As for the emulsion with surfactant concentration of 0.1 %wt, oil droplets rapidly coalesce when we drain the emulsion from the flow loop facility. Therefore, a clear image showing droplet size distribution cannot be captured under the optical microscope, which indicates that oil phase is not as fully emulsified as that of surfactant concentration being 0.25 %wt, and thus, the emulsion with surfactant concentration of 0.1 %wt possesses moderate stability. From Figure 3a, c, e, and g, we can see that oil droplets become smaller and their distribution presents more homogeneous with the increasing total flow velocity and this phenomenon proves that oil phase can be further emulsified under high total flow velocity. Besides, regarding Figure 3b, d, f, and h, it is notable that oil droplets exist with even smaller sizes at high water-cut due to less amount of oil. Hence, emulsion performs better stability under large water-cut as well as high total flow velocity.

Figure 4 exhibits the fluctuation signals of VMEA sensor at 0.1 %wt concentration of surfactant at different flow conditions. As can be seen, with the concentration of surfactant being 0.1 %wt, the water-cut set at 80 % and

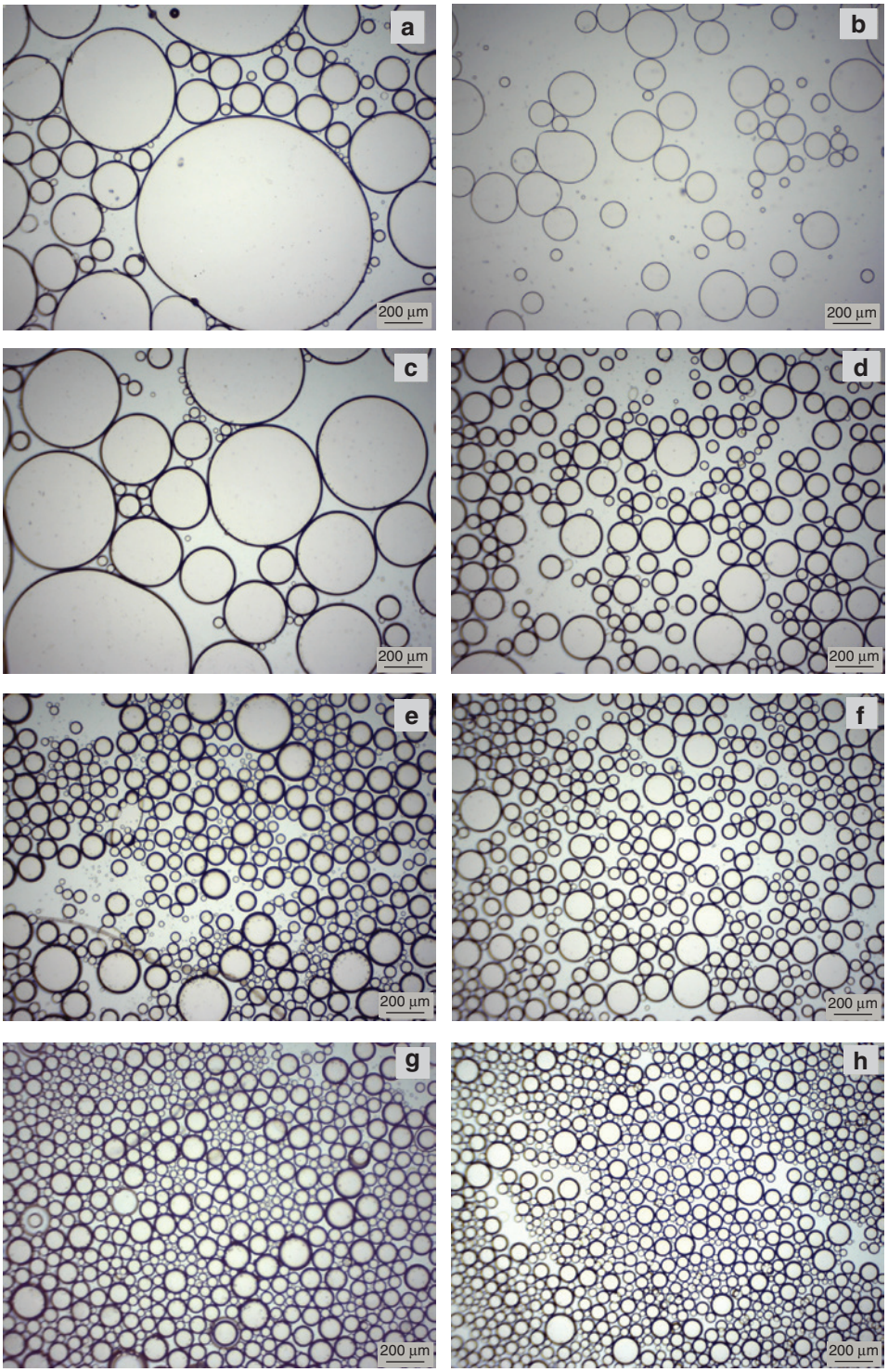

Figure 3: Optical microscopy images of emulsions with 0.25 %wt surfactant concentration at different water-cuts and total flow velocities: (a) $U_m = 0.0184$ m/s $K_w = 80$ %; (b) $U_m = 0.0184$ m/s $K_w = 96$ %; (c) $U_m = 0.0736$ m/s $K_w = 80$ %; (d) $U_m = 0.0736$ m/s $K_w = 96$ %; (e) $U_m = 0.1840$ m/s $K_w = 80$ %; (f) $U_m = 0.1840$ m/s $K_w = 96$ %; (g) $U_m = 0.2576$ m/s $K_w = 80$ %; (h) $U_m = 0.2576$ m/s $K_w = 96$ %.

the mixture velocity smaller than 0.1472 m/s, the fluctuating amplitude and frequency of voltage signals of VMEA sensor increases with the rising mixture velocity, indicating that under low mixture velocity, oil droplets in emulsion coalesce to form larger oil bubbles. When the oil bubbles flow through the measuring area, they will induce

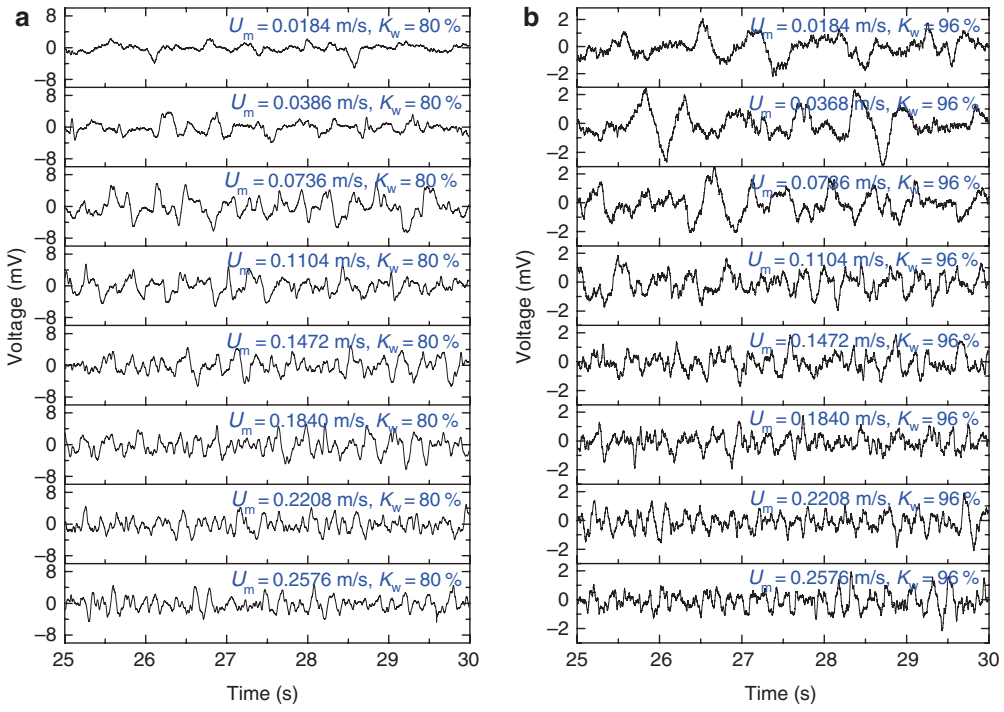

Figure 4: The signals of VMEA sensor at the 0.1 %wt concentration of SDBS.

larger fluctuating amplitude of sensor signals. Besides, the number of oil bubble increases with the increasing mixture velocity. As the total flow velocity exceeds 0.1472 m/s, the fluctuating amplitude of voltage signals of VMEA sensor presents a trend of decreasing gradually with the increasing mixture velocity, and the fluctuating frequency intensifies, which indicates that with the accelerating mixture fluid, the turbulent energy enhances and big oil bubbles are disintegrated to small oil droplets. Therefore, the fluctuating amplitude presents small when the oil droplets flow through the measuring area.

In addition, comparing Figure 4a and b, we find that the fluctuating amplitude is lower at high water-cut under the same mixture velocity and with the increasing mixture velocity, the fluctuating amplitude of signals seldom changes. The result implies that as there exists less oil phase in the pipe for higher water-cut, under the synergistic effect of surfactant and the turbulent energy of mixed fluid, oil bubbles are broken up into small oil droplets uniformly distributing in the pipe at low mixture velocity.

Figure 5 illustrates the fluctuation signals of VMEA sensor at 0.25 %wt concentration of surfactant under different flow conditions. Comparing Figures 4 and 5, we can conclude that the fluctuating amplitude presents lower at 0.25 %wt concentration of surfactant, which implies that the interfacial tension between oil and water is decreasing with the increasing of surfactant concentration. Oil phase is further emulsified and the oil droplets with smaller size distribute in the pipe homogeneously.

3 Recurrence Plot Analysis

RP analysis is a visualisation method which is based on phase space reconstruction of nonlinear dynamics to analyse recurrence characteristics of dynamic systems [30]. In previous researches, this method has been applied to classify the flow pattern of two-phase flow, and it is found that RP analysis can be an effective indicator of flow pattern identification [31, 32]. For a given original time series $\{x_1, x_2, \ldots x_n\}$, according to the embedding theory introduced by Takens [33] (m is embedding dimension and τ is delay time), the space vector and recurrence matrix are formulated as

$$\mathbf{X}_i = \{x_i, x_{i+\tau}, \ldots, x_{i+(m-1)\tau}\} \quad (i=1, 2, \ldots, N) \tag{1}$$

$$R_{i,j} = \Theta(\varepsilon - \|\mathbf{X}_i - \mathbf{X}_j\|), \quad i, j=1\ldots N \tag{2}$$

where N is the total number of points in phase space and $\|\cdot\|$ is Euclidean norm. $\Theta(\cdot)$ represents Heaviside function while $\varepsilon = r\delta$ is a predefined distance threshold. r and

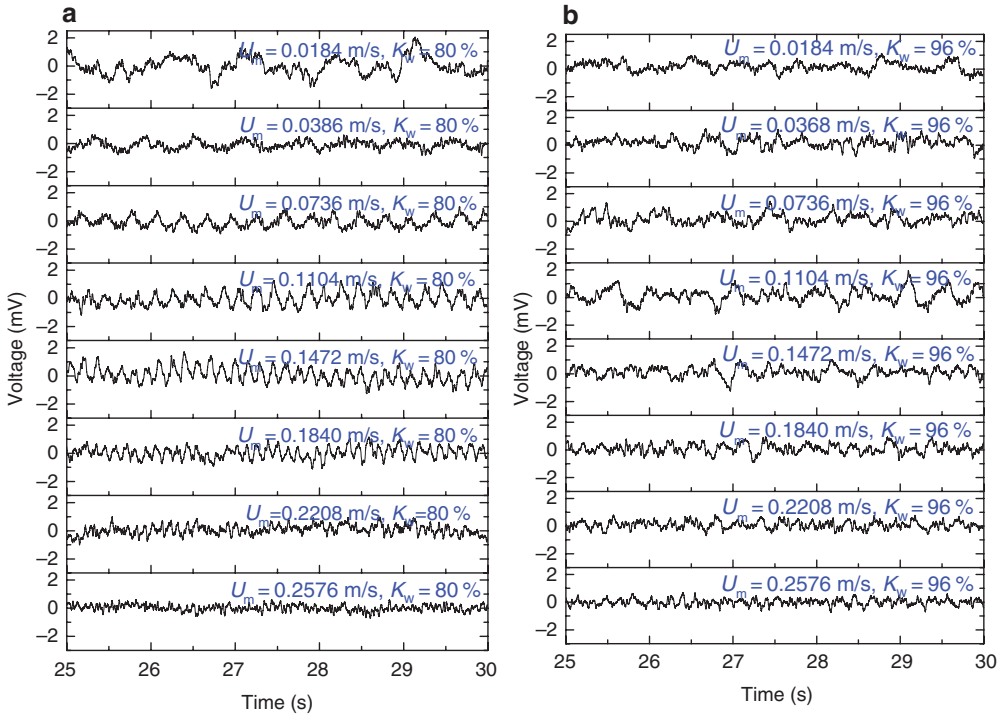

Figure 5: The signals of VMEA sensor at the 0.25 %wt concentration of SDBS.

δ are a predefined distance and the standard deviation of data, respectively. The values of $R_{i,j}$ only consist of 0 and 1. The graphical representation for RPs is composed of $N \times N$ points, which are marked black for 1 and white for 0. A black point in RP means that $\mathbf{X}_j$ lies in the inner space of the sphere with radius being ε, and this state is similar to $\mathbf{X}_i$.

Figures 6 and 7 show the RPs of oil-in-water emulsions with surfactant concentration being 0.1 %wt at different mixture velocities, with water-cut set 80 % and 96 %, respectively. There encompasses two subgraphs in each RP. The upper picture represents measurement signals of sensor, whereas the RP texture structure is shown below. It can be seen that from Figure 6, when the mixture velocities correspond to 0.0184 and 0.0736 m/s with the water-cut set at 80 %, the fluctuating frequency of signal is low, meanwhile the RP texture structure presents incomplete rectangular block structures, along with some scattered points. The results indicate that except for large oil bubbles, there also exist small oil droplets moving randomly in the testing pipe. When the mixture velocity is 0.1840 m/s, the fluctuating frequency of sensor signal increases and the RP texture structure gradually transforms into plenty of scattered points. As the mixture velocity reaches 0.2576 m/s, the RP texture structure almost evolves to scattered points. The results imply that large oil bubbles are gradually disintegrated to small oil droplets with random motion. Therefore, oil phase is further emulsified with increasing total flow velocity.

As shown in Figures 6 and 7, in contrast with the RP texture structure of water-cut with 80 %, the rectangular block structures of RP texture structure with water-cut being 96 % almost disappear, meanwhile the scattered points of water-cut being 96 % is more dispersive than those of water-cut with 80 % at the same total flow velocity. The results show that with higher water-cut, oil phase is easier to be broken up into smaller oil droplets moving upward randomly. Oil phase is easier to be emulsified at high water-cut.

Figures 8 and 9 exhibit the RPs of emulsions with surfactant concentration being 0.25 %wt at different mixture velocities, with water-cut set 80 % and 96 % respectively. Compare Figures 6–9, we find that when the concentration of surfactant is 0.25 %wt, only with mixture velocity being 0.0184 m/s and water-cut of 80 %, the RP texture structure possesses some regular textures. Furthermore, when the total flow velocity is >0.0736 m/s, the RP texture structure has already absolutely changed to scattered points. Compared to the results with 0.1 %wt surfactant concentration, oil phase has already been decomposed into smaller oil droplets at low flow velocities with 0.25 %wt

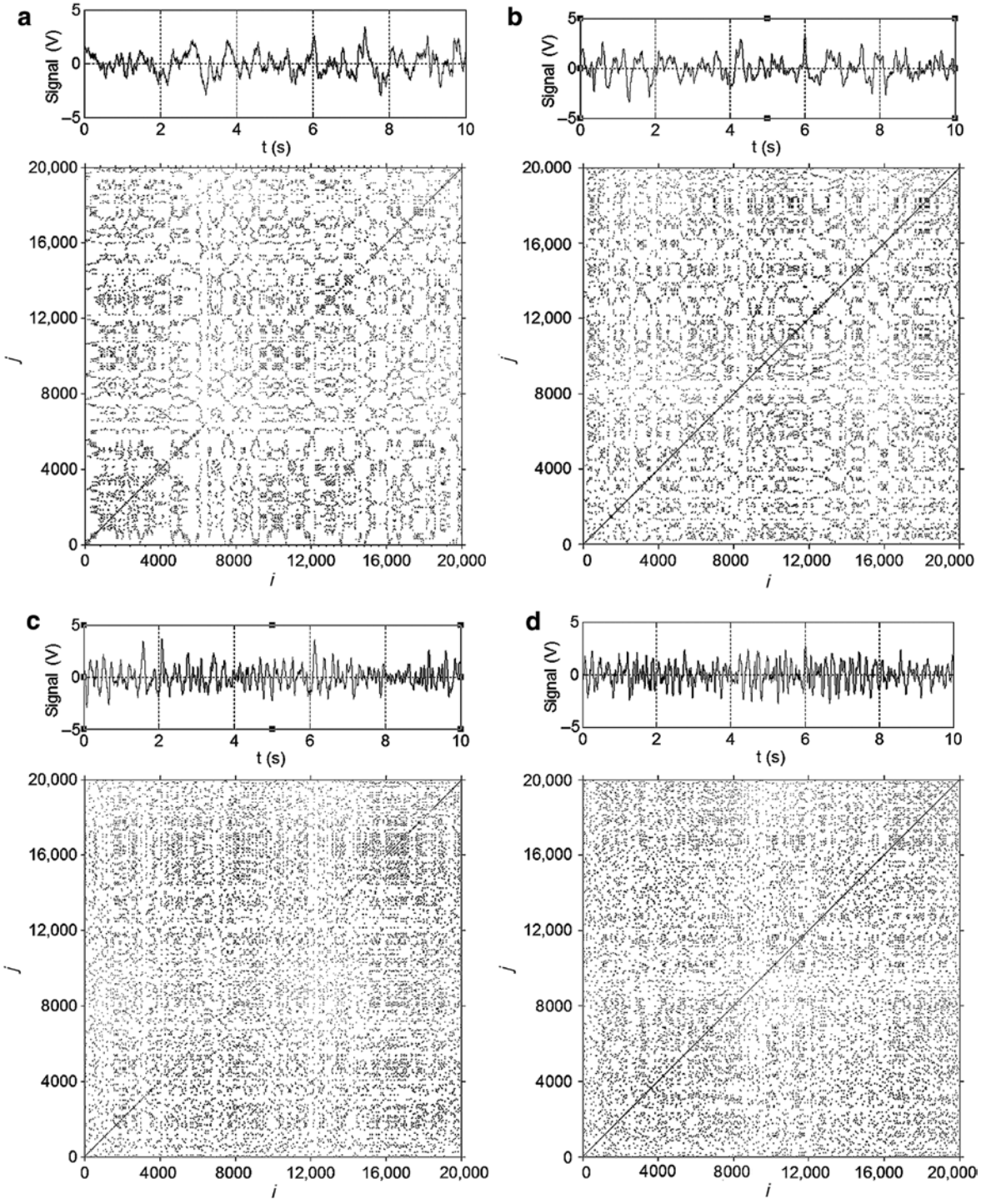

Figure 6: Recurrence plot of emulsions with surfactant concentration 0.1 %wt and water-cut 80 %: (a) $U_m = 0.0184$ m/s, (b) $U_m = 0.0736$ m/s, (c) $U_m = 0.1840$ m/s, and (d) $U_m = 0.2576$ m/s.

surfactant concentration. The results indicate that under higher surfactant concentration, as the interfacial tension between oil and water further decreases the oil phase can be readily broken up into smaller oil droplets. Besides, as shown in Figures 6d, 7d, 8d, and 9d, though all the RP texture structures exhibit scattered points at 0.2576 m/s, the scattered points are more dispersive at high surfactant concentration and high water-cut, when oil phase is further emulsified and oil-in-water emulsions present better stability.

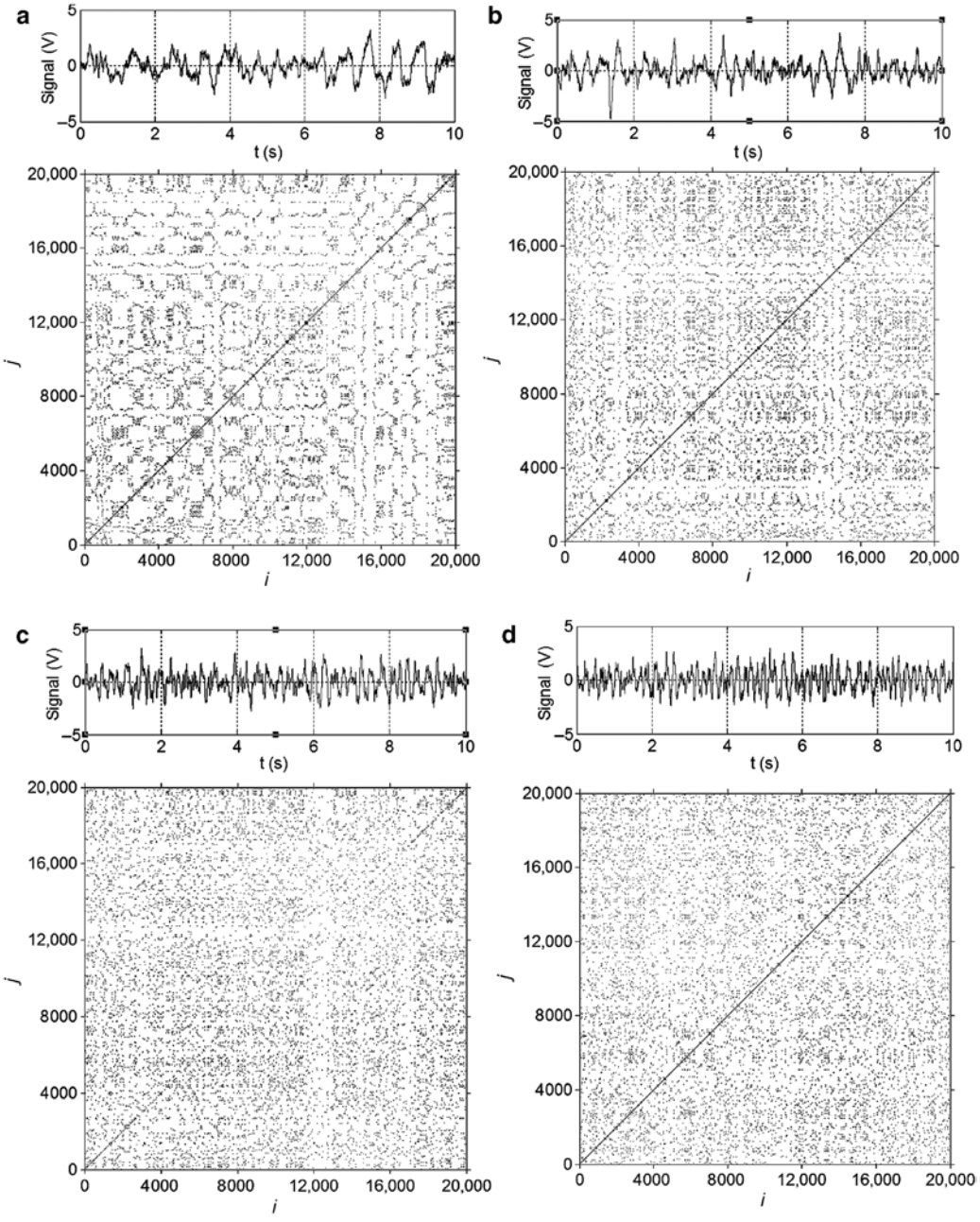

Figure 7: Recurrence plot of emulsions with surfactant concentration 0.1 %wt and water-cut 96 %: (a) $U_m = 0.0184$ m/s, (b) $U_m = 0.0736$ m/s, (c) $U_m = 0.1840$ m/s, and (d) $U_m = 0.2576$ m/s.

4 Multi-Scale Weighted Complexity Entropy Causality Plane (MS-WCECP)

4.1 MS-WCECP Theory

"Information H" and "disequilibrium Q" describe the complexity of a system from different perspectives: "Information H" shows the amount of information needed for describing the behavior of the system; "disequilibrium Q" represents the distance between a given probability distribution and the equilibrium probability distribution. The combination of "information H" and "disequilibrium Q" could be used as a measure of "statistical complexity C" [34]:

$$C = HQ \tag{3}$$

Through the values of H and Q, we can obtain corresponding statistical complexity measure C, which

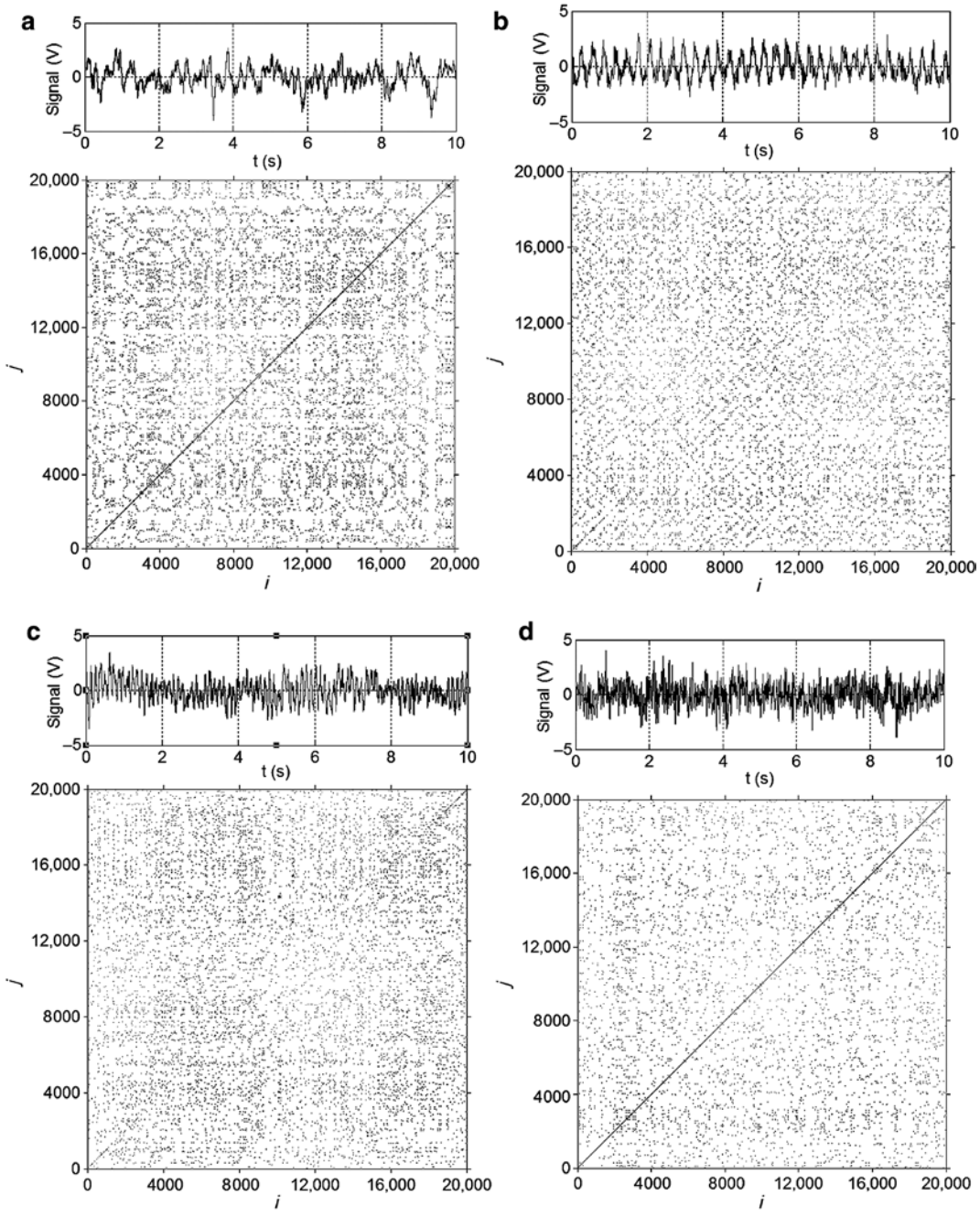

Figure 8: Recurrence plot of emulsions with surfactant concentration 0.25 %wt and water-cut 80 %: (a) $U_m = 0.0184$ m/s, (b) $U_m = 0.0736$ m/s, (c) $U_m = 0.1840$ m/s, and (d) $U_m = 0.2576$ m/s.

can reveal the hidden intrinsic mode of inside complex dynamic characteristics of system. The statistical complexity measure consists of LMC complexity measure [34], SDL complexity [35], and complexity measure C_{JS} introduced by Rosso et al. [26, 27, 36]:

$$C_{JS}[P] = Q_J[P, P_e] H_S[P] \tag{4}$$

where $Q_J[P, P_e]$ is the normalised Jensen–Shannon divergence and $H_S[P]$ represents the normalised permutation entropy [22]. Jensen–Shannon divergence can be defined as the distance between probability P and the equilibrium probability distribution P_e, which depicts the disequilibrium of a system, and it can be formulated as

$$Q_J[P, P_e] = Q_0 \{S[(P + P_e)/2] - S[P]/2 - S[P_e]/2\} \tag{5}$$

$$Q_0 = -2\left\{\left(\frac{m!+1}{m!}\ln(m!+1) - 2\ln(2m!) + \ln(m!)\right)\right\}^{-1} \tag{6}$$

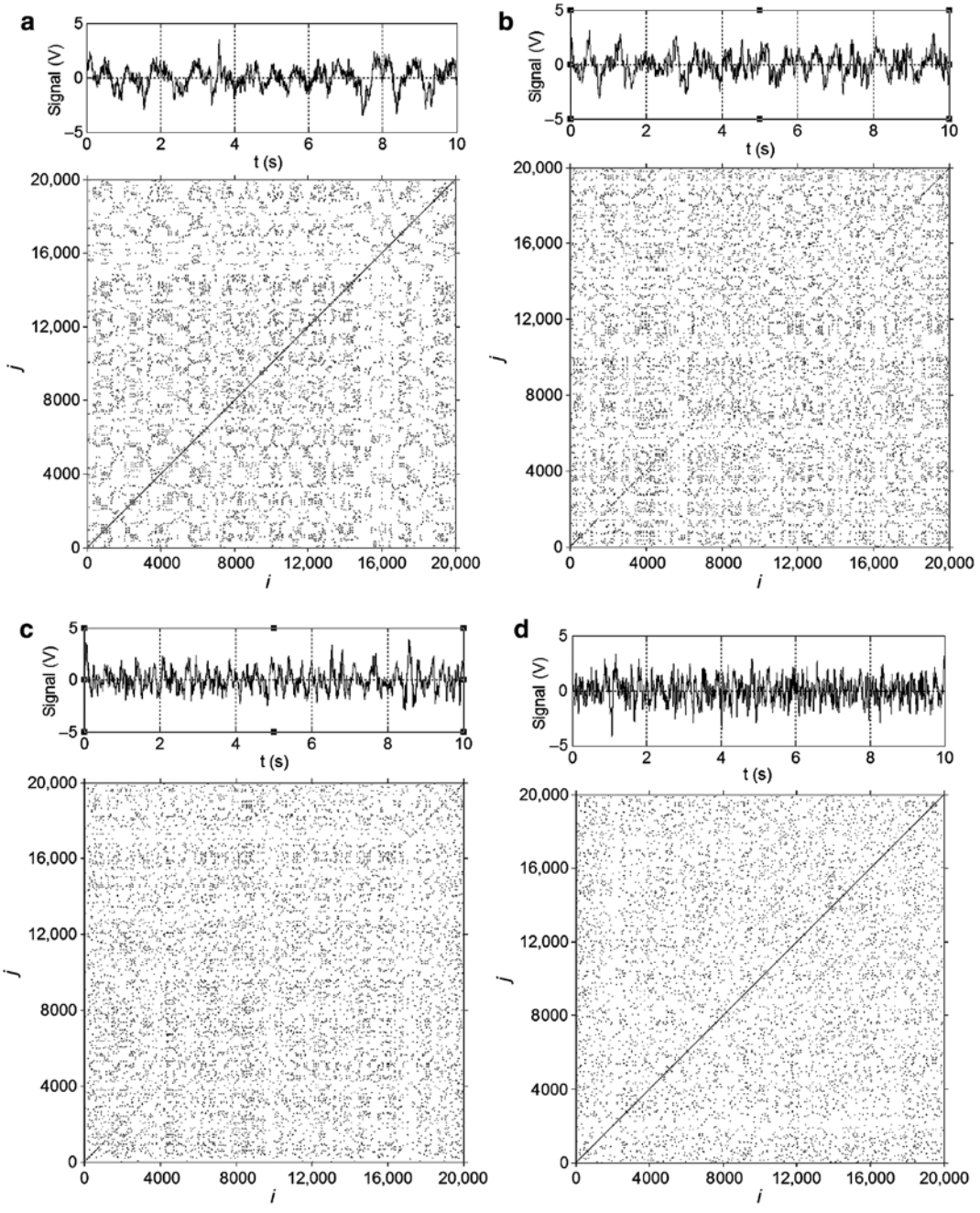

Figure 9: Recurrence plot of emulsions with surfactant concentration 0.25 %wt and water-cut 96 %: (a) $U_m = 0.0184$ m/s, (b) $U_m = 0.0736$ m/s, (c) $U_m = 0.1840$ m/s, and (d) $U_m = 0.2576$ m/s.

where Q_0 and m denote a normalised constant and embedding dimension, respectively. Through normalising weighted permutation entropy $S[P]$ by dividing $\ln(m!)$, the normalised weighted permutation entropy $H_w[P]$ [24] is obtained:

$$H_w[P]=S[P]/\ln(m!) \tag{7}$$

Thus, we could acquire a new complexity measure $C_w[P]$:

$$C_w[P]=Q_J[P,P_e]H_w[P] \tag{8}$$

Based on C–H plane introduced by Rosso et al. [26] and time series multi-scale coarse-grained analysis method [37], our research team has proposed multi-scale complexity entropy causality plane (MS-CECP) [28] and multi-scale weighted permutation entropy (MS-WPE) [25]. The steps of time series multi-scale coarse-grained

analysis method can be stated as follows: for a given time series $\{x(i), i=1, 2, \ldots, N\}$, reconstruct it to be a coarse-grained time series $\{y^s(j), j=1, 2, \ldots, N/s\}$ with the scale s. Where

$$y^s(j)=\frac{1}{s}\sum_{i=(j-1)s+1}^{js} x(i), \quad 1\le j\le N/s \tag{9}$$

In our previous study, Tang et al. [29] combined MS-CECP with MS-WCE and put forward the weighted complexity entropy causality plane (multi-scale weighted complexity entropy causality plane, shortened as MS-WCECP), where its horizontal axis and vertical axis are normalised weighted permutation entropy H_w and complexity measure C_w, respectively.

4.2 MS-WCECP Analysis of Typical Signal

Herein, the MS-WCECP is applied to analyse the time series $\{y_n\}$ of the Lorenz signal. The length of time series and the maximum coarse-grained scale are 10,000 and 60, respectively. We choose the embedding dimension $m=6$ and the time delay $\tau=1$. The equations of Lorenz are presented as follows:

$$\begin{cases}\dot{x}=\sigma(y-x)\\ \dot{y}=rx-y-xz\\ \dot{z}=xy-bz\end{cases} \tag{10}$$

where $\sigma=16$, $r=45.92$, $b=4$ and the initial value are set as $x=-1$, $y=0$, $z=1$. The time series $\{y_n\}$ of Lorenz signal is shown as Figure 10a and b represents corresponding MS-WCECP. With the increasing of coarse-grained scale, the correlation of sample points of the time series $\{y_n\}$ is gradually weakened, meanwhile the trajectory of MS-WCECP stretches from regular region to intricate region, and finally ends in noise region, which reflects the missing process of dynamic structure with the increasing of scale.

4.3 Nonlinear Dynamic Characteristics of Oil-in-Water Emulsions

Based on the fluctuation signals of VMEA sensor, the MS-WCECP is used to probe into the flow structure of oil-in-water emulsions under the addition of surfactant. We choose the embedding dimension m, the time delay τ, and the length of signal series are 6, 1, and 20,000, respectively.

Figure 11 exhibits the MS-WCECP of oil-in-water emulsions with 0.1 %wt surfactant concentration at different water-cuts and total flow velocities. Figure 11a, c, e, g, and i shows the MS-WCECP of oil-in-water emulsions with 0.1 %wt surfactant concentration with water-cuts being 80 %, 84 %, 88 %, 92 %, and 96 %, respectively. Figure 11b, d, f, h, and j is the values (intercept point) of H_w and C_w of Figure 11a, c, e, g, and i in the maximum scale. As shown in Figure 11, when the surfactant concentration is 0.1 %wt and the mixture velocity ranges from 0.0184 to 0.2576 m/s, the curves of MS-WCECP stop at intricate region with the increasing of coarse-grained scale. Furthermore, when the mixture velocity presents <0.1472 m/s, the intercept value of C_w in MS-WCECP gradually increases, which indicates the enhancing certainty of oil-in-water emulsions. The reason can be attributed to the fact that under low mixture velocity, oil droplets in emulsion coalesce and big oil bubbles take shape with the accelerating mixed fluid. When the mixture velocity further increases to 0.2576 m/s, the intercept value of C_w in MS-WCECP curves hardly changes, and the intercept point completely enters into the intricate region yet not fall into

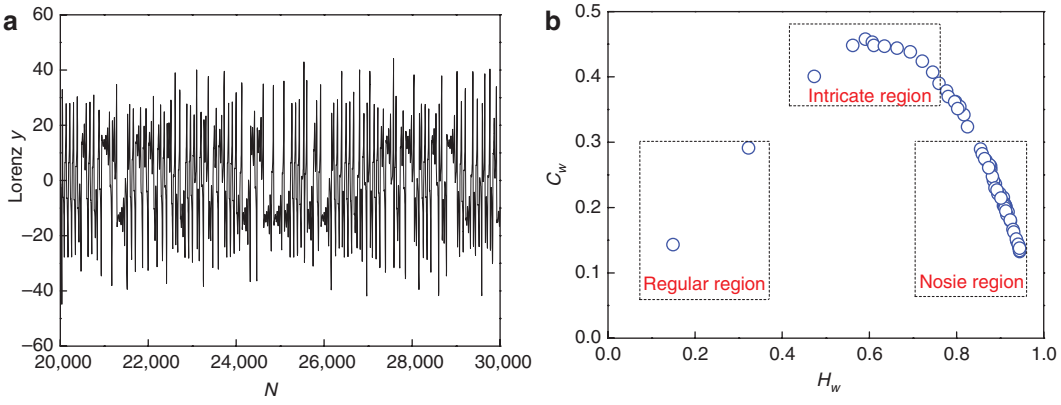

Figure 10: Time series $\{y_n\}$ of Lorenz signal and its MS-WCECP: (a) the time series $\{y_n\}$ of Lorenz signal and (b) MS-WCECP of $\{y_n\}$.

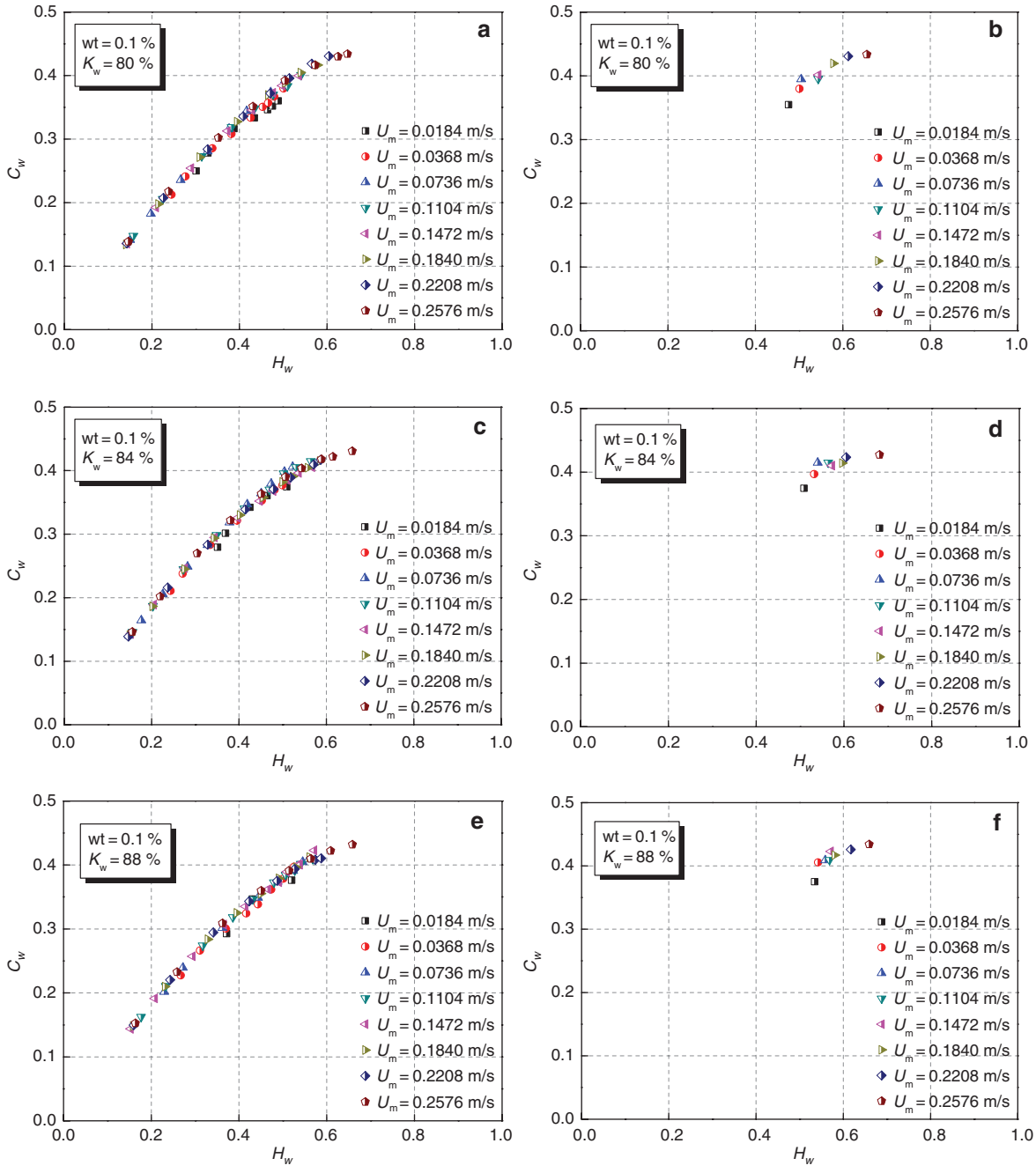

Figure 11: MS-WCECP of emulsions with 0.1 %wt surfactant concentration at different water-cuts and total flow velocities.

the noise area, which manifests that the emulsification degree of oil-in-water emulsions is not sufficient at low surfactant concentration.

Figure 12 delineates the MS-WCECP of oil-in-water emulsions with surfactant concentration of 0.25 %wt at different water-cuts and total flow velocities. Figure 12a, c, e, g, and i shows the MS-WCECP of oil-in-water emulsions with surfactant concentration of 0.25 %wt with water-cuts of 80 %, 84 %, 88 %, 92 %, and 96 %, respectively. Figure 12b, d, f, h, and j is the values (intercept point) of H_w and C_w of Figure 12a, c, e, g, and i in the maximum scale. As shown in Figure 12, when the surfactant concentration is 0.25 %wt, the intercept points of MS-WCECP curves mostly locate at intricate region under low mixture velocity, indicating that the distribution of dispersed oil droplets still possess some inherent certainty at this time. As the mixture velocity increases, the corresponding curves of MS-WCECP present disparate falling degrees with the increasing coarse-grained scale. Furthermore, the falling degree of curves becomes deeper with the increasing total

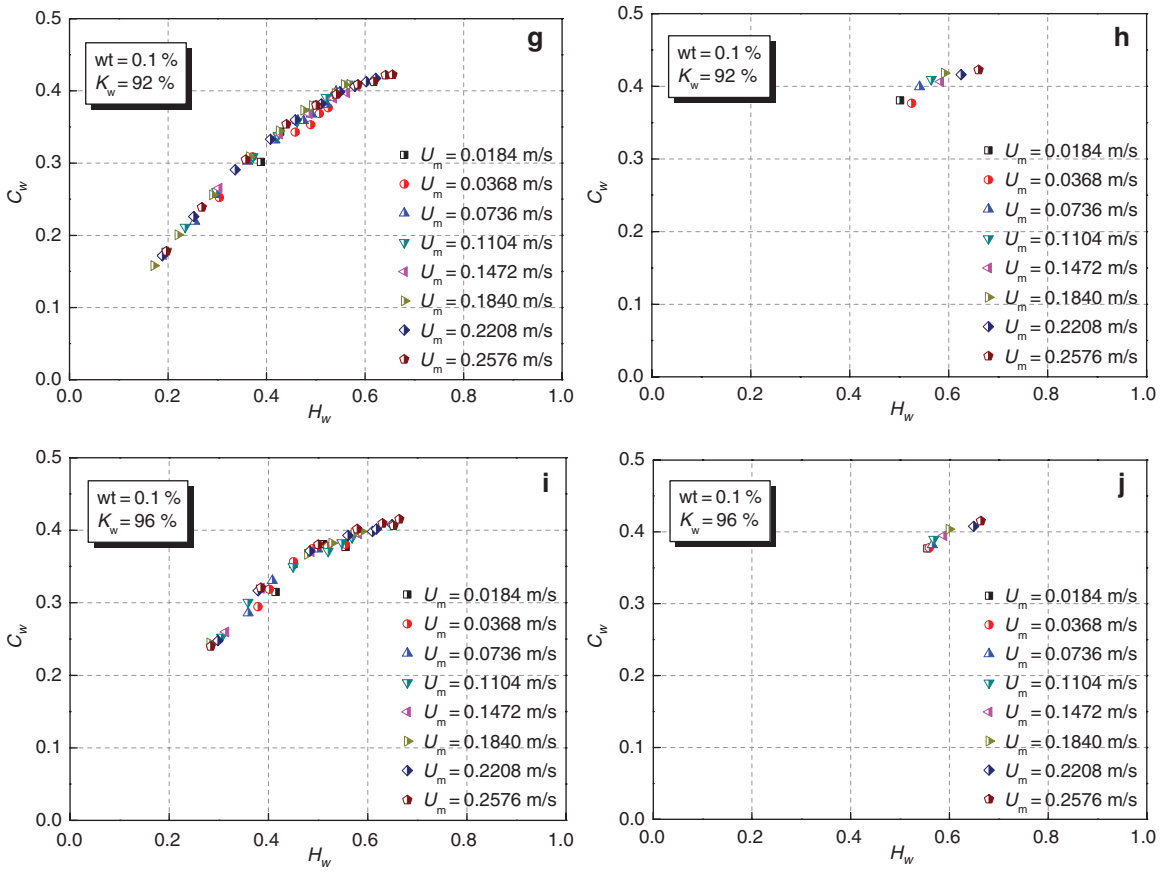

Figure 11 (continued)

flow velocities, and the intercept points present the tendency that moving from intricate region to noise region. It can be pinpointed that the certainty of oil phase gradually weakens, while the randomness of oil phase is gradually stronger with the increasing mixture velocity at this time, and emulsification degree of oil-in-water emulsions is more sufficient.

As shown in Figure 12b, d, f, h, and j, when the total flow velocity is 0.2576 m/s, the falling degree of curves become larger and the intercept points present the tendency of stretching from intricate region to noise region of MS-WCECP with increasing water-cut. It can be inferred that when the surfactant concentration is 0.25 %wt, the randomness of oil phase is gradually stronger, meanwhile the degree of emulsification of the oil phase is more adequate, and the motion of oil droplets finally presents completely random state with the increment of water-cut. Thereby, the oil phase is further emulsified in the end in comparison with that of surfactant concentration being 0.1 %wt.

Through comparing Figure 11 with Figure 12, it can be seen that all the intercept points of MS-WCECP are located at intricate region and the emulsions present higher certainty with the surfactant concentration of 0.1 %wt. However, when the surfactant concentration is equal to 0.25 %wt, as it can more effectively reduces the oil-water interfacial tension, all the curves of MS-WCECP stretches from regular region to intricate region, and finally ends in noise region, meanwhile the intercept points move from intricate region to noise region with the increasing mixture velocity, indicating the further emulsion of oil phase, and the oil-in-water emulsions show more obvious random movement characteristic.

The effect of the concentration of surfactant on the droplet size in emulsion has been widely reported. Nesterenko et al. [4] set an particles/surfactant system to investigate the synergic stabilisation of water-in-oil emulsion and concluded that the droplet size of dispersed phase is decreasing as surfactant concentration increases at a fixed particle concentration due to the decreasing of interfacial tension between oil and water. Tcholakova et al. [38, 39] studied the influence of different types of emulsifier on the mean drop size during emulsification and found that in the surfactant-poor regime, the mean drop size decreases

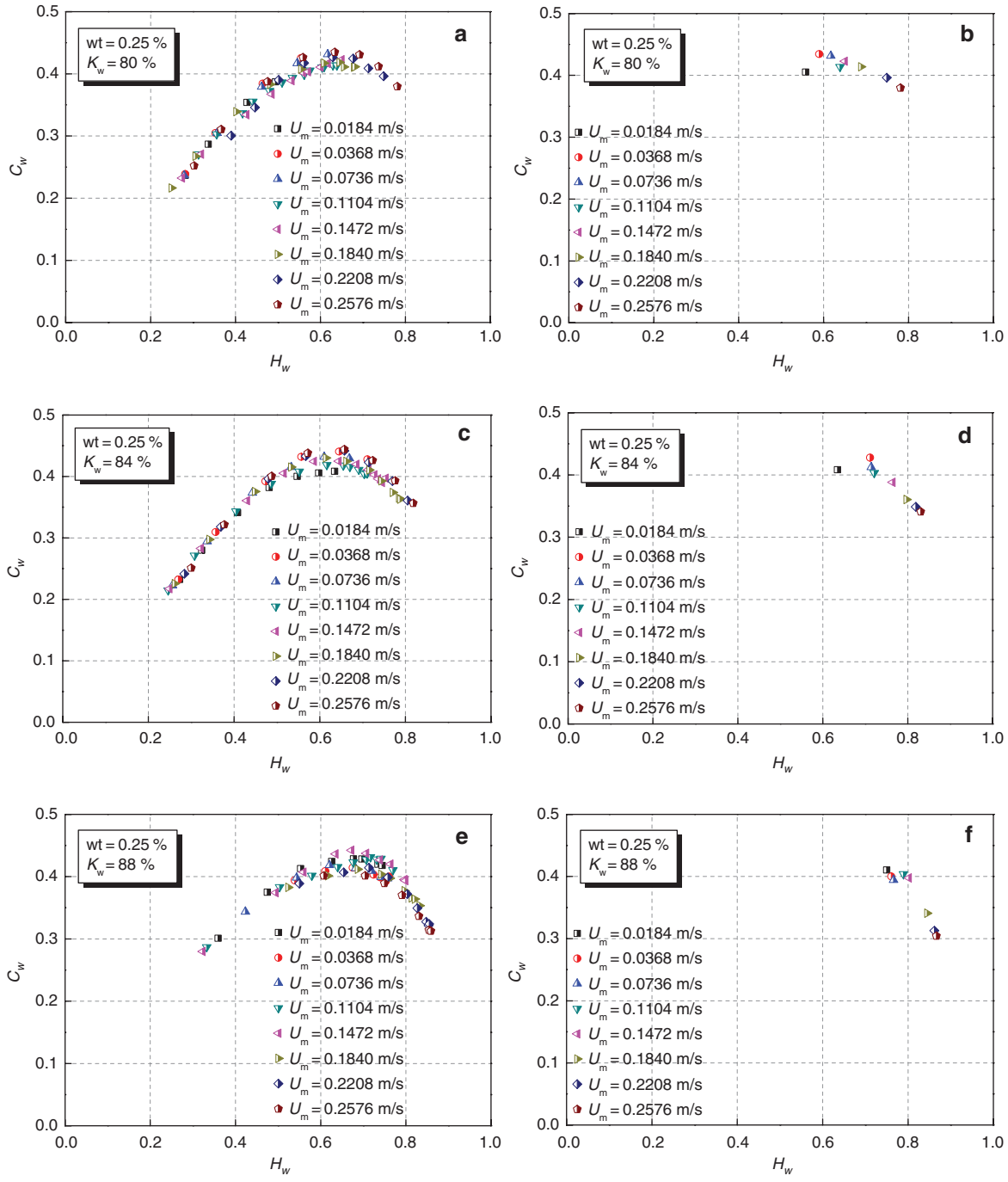

Figure 12: MS-WCECP of emulsions with 0.25 %wt surfactant concentration at different water-cuts and total flow velocities.

significantly with the increase in emulsifier concentration, while the mean drop size does not depend on the emulsifier concentration in the surfactant-rich regime. This study analysed the effect of surfactant concentration, water-cut, and total flow velocity on the oil-in-water emulsions in the vertical upward pipeline flow from the perspective of nonlinear dynamic characteristics, and our conclusions show good agreement to the previous studies.

5 Conclusions

The measurement signals of vertical VMEA sensor, RP algorithm, and multi-scale weighted complexity entropy causality plane (MS-WCECP) are used to investigate the nonlinear dynamic characteristics of oil-in-water emulsions under the addition of surfactant in this article. To sum up, the conclusions are stated as follows:

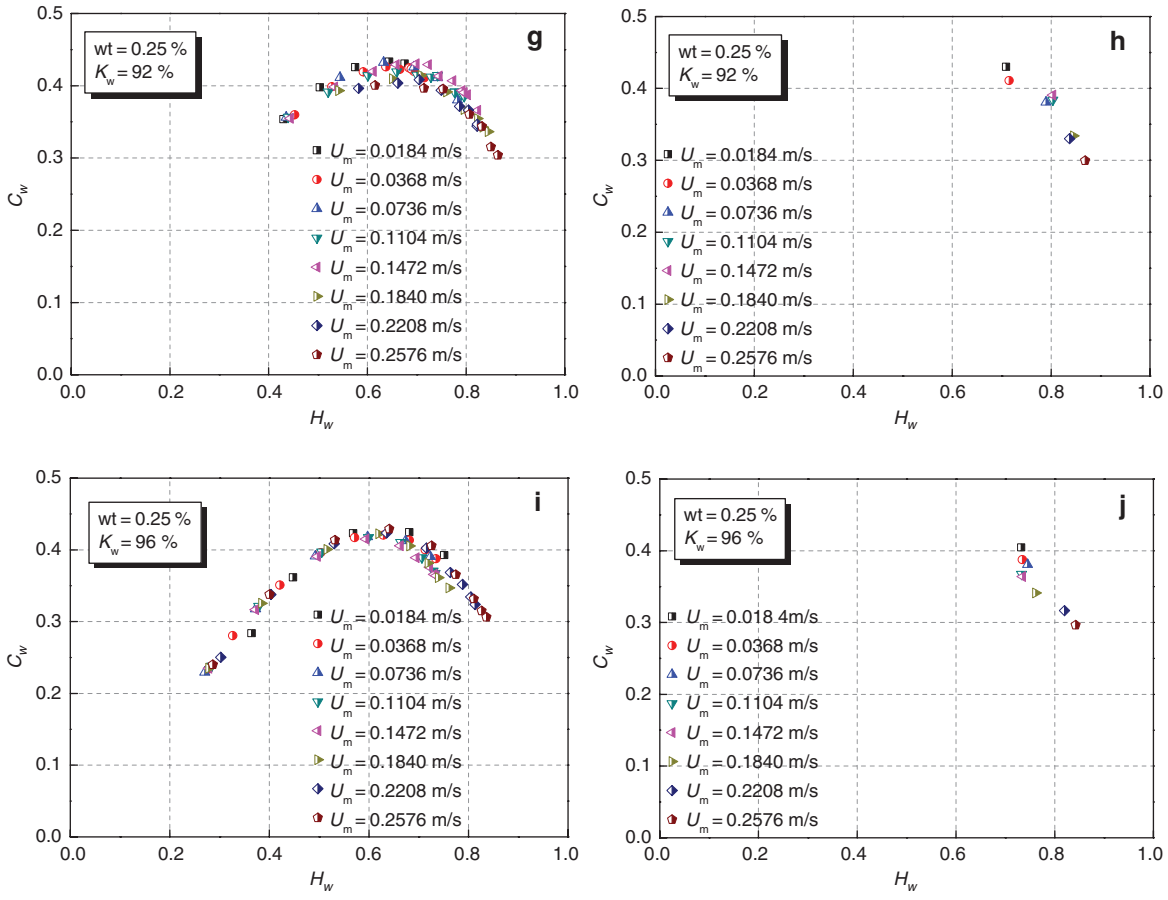

Figure 12 (continued)

1. The RP algorithm was applied to study the oil-in-water emulsions under the addition of surfactant. The results present that the randomness of oil phase becomes higher with the increasing mixture velocity. Furthermore, random motion of oil phase is more obvious at high water-cut. For identical flow conditions, the scattered points of RP at high surfactant concentration are more dispersive, indicating that the oil phase is further emulsified and oil-in-water emulsions present better stability at high surfactant concentration and high water-cut.
2. The multi-scale weighted complexity entropy causality plane (MS-WCECP) was used to analyse the complexity and randomness of oil-in-water emulsions flow structure. When the surfactant concentration is 0.1 %wt, the intercept points of MS-WCECP are located at intricate region, and the oil-in-water emulsions possess some certainty at this time. However, when the surfactant concentration is 0.25 %wt, the intercept points of MS-WCECP are situated at noise region and the emulsions absolutely enter into a random state, indicating that the oil phase is completely emulsified and the emulsions present better stability, which coincides with the conclusions from RP algorithm.

Acknowledgments: This study was supported by the National Natural Science Foundation of China (Grant Nos. 11572220, 51527805).

References

[1] T. Roques-Carmes, H. Monnier, J. F. Portha, P. Marchal, and L. Falk, Chem. Eng. Res. Des. **92**, 2758 (2014).
[2] A. Salonen, R. Lhermerout, E. Rio, D. Langevin, and A. Saint-Jalmes, Soft Matter **8**, 699 (2011).
[3] T. Krebs, K. Schroën, and R. Boom, Soft Matter **8**, 10650 (2012).
[4] A. Nesterenko, A. Drelich, H. Lu, D. Clausse, and I. Pezron, Colloids Surf. A **457**, 49 (2014).
[5] A. Pizzino, M. Catté, E. V. Hecke, J. L. Salager, and J. M. Aubry, Colloids Surf. A **338**, 148 (2009).
[6] C. P. Aichele, M. Flaum, T. Jiang, G. J. Hirasaki, and W. G. Chapman, J. Colloid Interf. Sci. **315**, 607 (2007).
[7] N. Malassagne-Bulgarelli and K. M. McGrath, Soft Matter **9**, 48 (2012).

[8] Z. C. Li, H. R. Liu, L. Zeng, H. W. Liu, S. Yang, et al., Langmuir **30**, 12154 (2014).
[9] P. Kundu, A. Agrawal, H. Mateen, and I. M. Mishra, Chem. Eng. Sci. **102**, 176 (2013).
[10] Z. X. Dong, M. Q. Lin, H. Wang, and M. Y. Li, Petrol. Sci. **2**, 263 (2010).
[11] C. D. Ampatzidis, E. M. A. Varka, and T. D. Karapantsios, Colloids Surf. A **460**, 176 (2014).
[12] E. Santini, E. Guzmán, M. Ferrari, and L. Liggieri, Colloids Surf. A **460**, 333 (2014).
[13] J. S. Sander, L. Isa, P. A. Ruhs, P. Fischer, and A. R. Studart, Soft Matter **8**, 11471 (2012).
[14] J. Miras, S. Vílchez, C. Solans, T. Tadros, and J. Esquena, Soft Matter **9**, 8678 (2013).
[15] R. Covis, E. Marie, and D. Alain, Am. Inst. Chem. Eng. J. **61**, 277 (2015).
[16] W. L. Kang, B. Xu, Y. J. Wang, Y. Li, X. H. Shan, et al., Colloids Surf. A **384**, 555 (2011).
[17] L. Liu, X. Li, L. Tong, and Y. Liu, J. Petrol. Sci. Eng. **115**, 1 (2014).
[18] A. T. V. Nimwegen, L. M. Portela, and R. A. W. M. Henkes, Int. J. Multiphas. Flow **71**, 133 (2015).
[19] A. T. V. Nimwegen, L. M. Portela, and R. A. W. M. Henkes, Int. J. Multiphas. Flow **71**, 146 (2015).
[20] A. T. V. Nimwegen, L. M. Portela, and R. A. W. M. Henkes, Int. J. Multiphas. Flow **78**, 132 (2016).
[21] M. Al-Yaari, A. Al-Sarkhi, I. A. Hussein, F. Chang, and M. Abbad, Chem. Eng. Res. Des. **92**, 405 (2014).
[22] C. Bandt and B. Pompe, Phys. Rev. Lett. **88**, 174102 (2002).
[23] L. Zunino, M. Zanin, B. M. Tabak, D. G. Pérez, and O. A. Rosso, Phys. A **388**, 2854 (2009).
[24] B. Fadlallah, B. Chen, A. Keil, and J. Principe, Phys. Rev. E **87**, 788 (2013).
[25] X. Chen, N. D. Jin, A. Zhao, Z. K. Gao, and L. S. Zhai, Physica A **417**, 230 (2015).
[26] O. A. Rosso, H. A. Larrondo, M. T. Martin, A. Plastino, and M. A. Fuentes, Phys. Rev. Lett. **99**, 12505 (2007).
[27] M. T. Martin, A. Plastino, and O. A. Rosso, Phys. Lett. A **311**, 126 (2003).
[28] F. X. Dou, N. D. Jin, C. L. Fan, Z. K. Gao, and B. Sun, Chin. Phys. B **23**, 120502 (2014).
[29] Y. Tang, A. Zhao, Y. Y. Ren, F. X. Dou, and N. D. Jin, Physica A **449**, 324 (2016).
[30] J. P. Eckmann, S. O. Kamphorst, and D. Ruelle, Europhys. Lett. **4**, 973 (1987).
[31] Y. B. Zong and N. D. Jin, Europ. Phys. J. Spec. Topics **164**, 165 (2008).
[32] Y. B. Zong, N. D. Jin, Z. Y. Wang, Z. K. Gao, and C. Wang, Int. J. Multiphas. Flow **36**, 166 (2010).
[33] F. Takens, Lect. Notes Math. **898**, 366 (1981).
[34] R. Lopez-Ruiz, H. L. Mancini, and X. Calbet, Phys. Lett. A **209**, 321 (1995).
[35] J. S. Shiner, M. Davison, and P. T. Landsberg, Phys. Rev. E **59**, 1459 (1999).
[36] P. W. Lamberti, M. T. Martin, A. Plastino, and O. A. Rosso, Physica A **334**, 119 (2004).
[37] M. Costa, A. L. Goldberger, and C. K. Peng, Phys. Rev. Lett. **89**, 705 (2002).
[38] S. Tcholakova, N. D. Denkov, D. Sidzhakova, I. B. Ivanov, and B. Campbell, Langmuir **19**, 5640 (2003).
[39] S. Tcholakova, N. D. Denkov, and T. Danner, Langmuir **20**, 7444 (2004).